Hindawi
Geofluids
Volume 2020, Article ID 8845250, 18 pages
https://doi.org/10.1155/2020/8845250

Research Article

A Model for a Multistage Fractured Horizontal Well with Rectangular SRV in a Shale Gas Reservoir

Jianfa Wu, Jian Zhang, Cheng Chang, Weiyang Xie, and Tianpeng Wu

PetroChina Southwest Oil & Gas Field Co., Chengdu, Sichuan, China

Correspondence should be addressed to Weiyang Xie; johnhatteras@163.com

Received 27 March 2020; Revised 12 October 2020; Accepted 20 October 2020; Published 7 December 2020

Academic Editor: Wen-Dong Wang

Although great success has been achieved in the shale gas industry, accurate production dynamic analyses is still a challenging task. Long horizontal wells coupling with mass hydraulic fracturing has become a necessary technique to extract shale gas efficiently. In this paper, a comprehensive mathematical model of a multiple fractured horizontal well (MFHW) in a rectangular drainage area with a rectangular stimulated reservoir volume (SRV) has been established, based on the conceptual model of "tri-pores" in shale gas reservoirs. Dimensionless treatment and Laplace transformation were employed in the modeling process, while the boundary element method was used to solve the mathematical model. The Stehfest numerical inversion method and computer programing techniques were employed to obtain dimensionless type curves, production rate, and cumulative production. Results suggest that 9 flow stages can be observed from the pseudopressure derivative type curve when the reservoir and the SRV are large enough. The number of fractures, SRV permeability, and reservoir permeability have no effect on the total production when the well is abandoned. As SRV and reservoir permeability increases, the production rate is much higher in the middle production stage. Although the SRV scale and its permeability are very important for early and intermediate production rates, the key factors restricting the shale gas production rate are the properties of the shale itself, such as adsorbed gas content, natural fractures, and organic content. The proposed model is useful for analyzing production dynamics with stimulated horizontal wells in shale gas reservoirs.

1. Introduction

Shale gas, together with coalbed methane, which was once the source rock of oil and gas. Shale gas is a typical unconventional gas stored with adsorbed, free gas ([1]; Li Yong et al., 2019). Shale gas consists mainly of methane, and there are many kinds of interlayers in shale strata, such as siltstone, silty mudstone, and politic siltstone. Currently, shale gas extraction is developing rapidly and has played an important role in the US energy industry since 2000. It has spread quickly to China and Australia as a potential energy source [2]. For example, the annual production of shale gas in 2007 in the US was 56.4 billion cubic meters, while it reached 447.0 billion cubic meters in 2016; its proportion to the world annual production is 12% [3]. With the success of shale gas development, shale gas has the potential to become the primary energy source in the future.

Due to the special formation characteristics and pore types of a shale gas reservoir, exploiting shale gas requires hydraulic fracturing. Specifically, i.e., horizontal wells with massive hydraulic fracturing [4–6]. Massive hydraulic fracturing of horizontal wells in shale gas reservoirs creates a fracture network around the well called stimulated reservoir volume (SRV). The SRV, which is the main method of increasing shale gas production, consists of hydraulic fractures and a fracture network. Therefore, it is important to devise an effective and accurate model to describe the SRV and to help understand the flow characteristics of shale gas underground.

Kucuk and Sawyer [7] proposed a model to analyze the adsorption and desorption characteristics in fractured reservoirs and derived a numerical solution to the model considering the effects of desorption and slippage. Lancaster and Gatens III [8] analyzed postfractured well testing data of

eastern Devonian shale, which was described as a dual-porosity reservoir, and those data were used to estimate fracture length and fracture conductivity. Devonian shale wells showed that fracture half-lengths calculated from conventional postfracture pressure-buildup tests were shorter than designed, based on which Johnston and Lee [9] proposed a new method to determine net pay thickness and presented results suggesting that conventional tests of those wells are inadequate.

Brown et al. [10] and Ozkan et al. [11] assumed that the main flow type in fractured horizontal wells is linear, and established a trilinear flow model for a multistage fractured horizontal well in a shale gas reservoir using the model presented by Lee and Brockenbrough (Lee and Brockenbrough 1986). Based on the linear-flow theory, a plate dual-porosity model, and the Warren-Root block dual-porosity model, Bello and Watenbargen [12] and Al-Ahmadi et al. [13] proposed a model to analyze the production dynamics and pressures of MFHWs in shale gas reservoirs. Nobakht et al. (Nobakht et al., 2012) first proposed the conceptual model of different combinations of horizontal wells, porous media types, and hydraulic fractures in shale gas reservoirs, and then analyzed the different flow stages during the development process. Assuming SRV exists only in a limited region around the fractures and fracture half-lengths equal to the width of the reservoir, Stalgorova and Mattar [14] derived a modified trilinear flow model and obtained the solution of this model in Laplace space. Xu et al. [15] proposed an unsteady seepage model of a MFHW at constant rate production in a shale gas reservoir. The model assumed that the flow types in a fractured horizontal well are alternately linear and transitional, and the fracture network exists in a limited region around the hydraulic fractures.

To summarize, there are two types of models to analyze well production performance of MFHWs with SRVs in shale gas reservoirs. One is the linear flow model, which is based on the assumption that all fractures have the same length and conductivity and are spaced uniformly along the horizontal well ([11–21]; Zhao et al., 2016b; [22–25]), and the main related schematics of linear models are listed in Table 1. Although it is common field practice to design equally spaced hydraulic fractures, the requirements of equal properties and fracture lengths of shale gas reservoirs are hard to satisfy because of the development of natural fractures and their anisotropy and heterogeneity. The other type of flow model is the numerical simulation model based on finite-element, finite-difference, or other numerical methods [26–36].

Normal shale gas reservoirs have a dual-porosity nature, with macropores and micropores in matrix, and microfractures made by hydraulic fracturing (Ge & Zhang, 2012; [38–40]). The output process of shale gas from the reservoir can be subdivided into 4 stages: (1) the gas desorbed from the matrix particle surfaces, (2) diffusion from the matrix to the macropores, (3) flows from the macropores to the microfractures, and (4) Darcy flows through the fracture network to the bottom hole.

Well testing analysis is an important dynamic monitoring tool for petroleum engineers to accurately determine the parameters of oil and gas reservoir engineering, to evaluate the stimulation in the shale gas reservoir, and to provide more effective plans for the oil field. In addition, a suitable mathematical model for horizontal wells with SRVs in shale gas reservoirs is vital to well testing.

As we can see from the above discussion, both analytical methods and linear flow models have their own deficiencies in obtaining production dynamics in shale gas reservoirs. On one side, analytical methods, such as point source and Green's function method, can only deal with seepage problems of shale gas in regular-shaped reservoirs, such as reservoirs with circular or infinite outer boundaries. However, the practical boundary of shale gas reservoirs is quite complex considering the effects of SRV, which in consequence cannot be handled by this traditional analytical method. On the other, linear flow models usually put the whole reservoir as a rectangular area, and subdivide the reservoir region into some small rectangular areas, as shown in Table 1. The subdivision principle of the small rectangular sections is the gas flow capacities in formations, i.e., a bigger flow capacity in the SRV region and a weaker flow capacity as the region. In linear flow models, a quarter of the area around a hydraulic fracture is usually studied for simplicity, which brings into another assumption that all hydraulic fractures are uniformly spaced and with the same length. These assumptions are also not in accordance with practical conditions of shale gas reservoirs. Besides, other flow patterns, such as redial flow and elliptical flow, and interferences among fractures cannot be reflected from the linear flow models. Thus, a more comprehensive and accurate model considering both the rectangular composite nature of a shale gas reservoir and the fracture heterogeneities need to be established in an effort to analyze production dynamics better in shale gas reservoirs. In this paper, we present a percolation model for a multistage horizontal well in a rectangular shale gas reservoir with an SRV considering unsteady transport theory, which cannot be tackled by analytical methods or linear flow conceptions. The boundary element method is employed to solve the proposed mathematical model, with parameter sensitivity analysis conducted for production dynamics. Results show that the model we propose should be useful for analyzing stimulated horizontal wells in shale gas reservoirs.

2. Transport Mechanism of Shale Gas

2.1. Characteristics of Shale Gas Reservoir. The characteristics of a shale gas reservoir are very different from those of a conventional gas well, in both the structure and the flow mechanism. The typical classification method is that of Loucks et al. [41]. They classified the pore types of the shale matrix and the natural microfractures; their classification is comprised of the following 4 types: intergranular pores, intragranular pores, organic pores, and natural microfractures (Figure 1 shows the main pore types of a shale gas reservoir). The first 2 pore types are related to the mineral grains. The difference between them is that intergranular pores develop between grains and intragranular pores develop within grains. Organic pores are intrapores of organic matter. In shale, the main pores are micropores, nanopores, and microfractures, so approximately 20% to 80% of the gas is absorbed by the

Table 1: Schematics of the linear models.

No.	Schematics of physical models	References
1	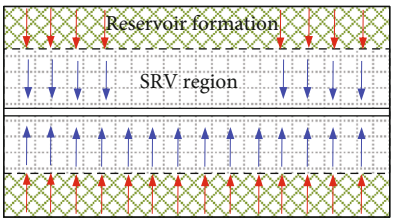	Xu et al. 2013 [15]
2	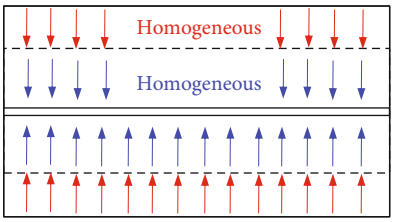	Nobakht and Clarkson 2013 [18]
3	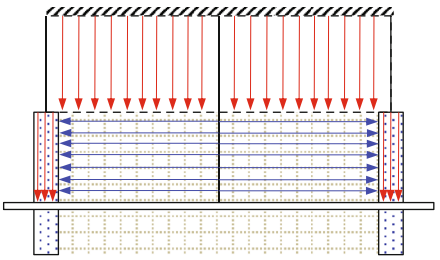	Brown et al. 2009 [10] Ozkan et al. 2013 [11]
4	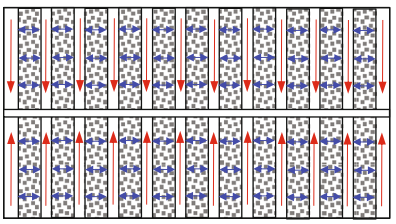	Bello and Wattenbarger (2010)
5	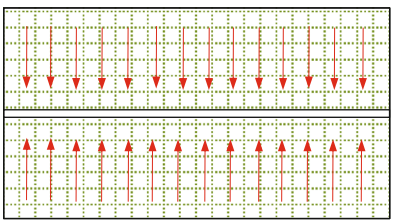	Al-Ahmadi et al. 2010 [13]
6	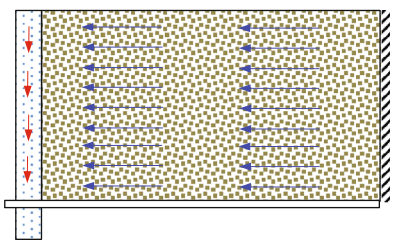	Nobakht et al. 2013 [19] Yao et al. 2013 [37]

Table 1: Continued.

No.	Schematics of physical models	References
7	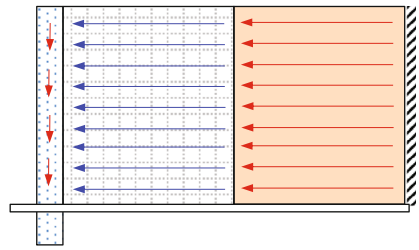	Stalgorova and Mattar 2012 [14]
8	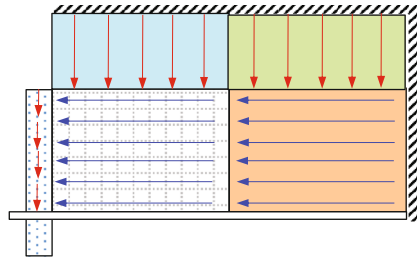	Stalgorova and Mattar 2013 [21]

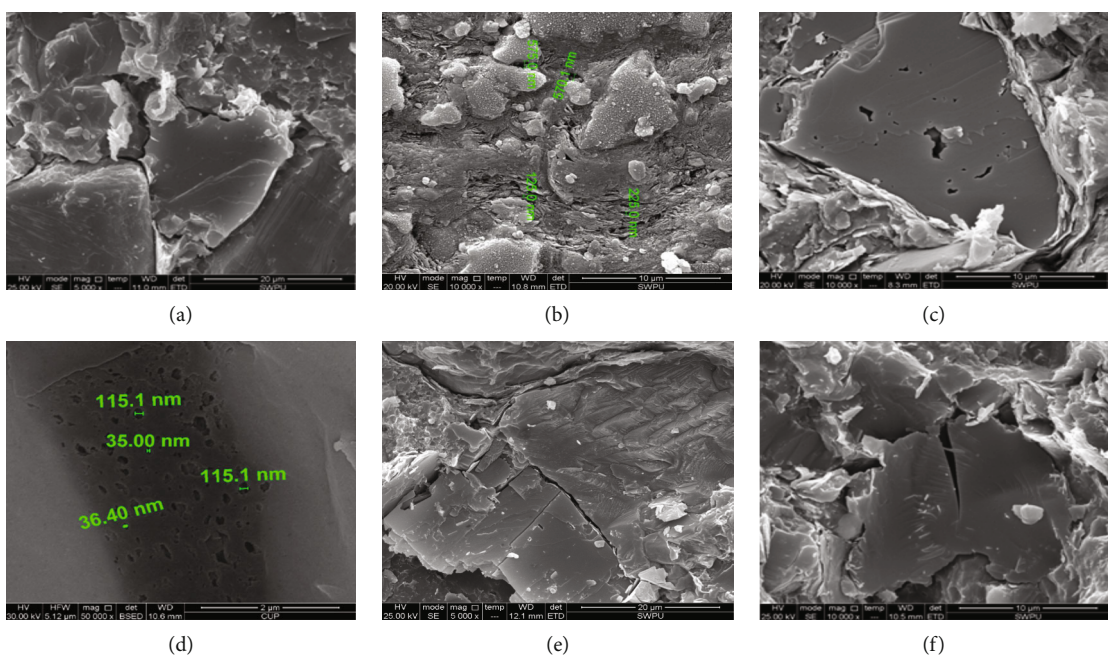

Figure 1: Main pore and fracture types in a shale gas reservoir. (a) Inorganic pores (intergranular pores). (b) Inorganic pores (intercrystalline pores). (c) Inorganic pores (intragranular dissolved pores). (d) Organic pores. (e) Cleavage fractures. (f) Intergranular fractures.

particles in the matrix, and the rest is free in the microfractures. Gas flow behaviors in shale nanopores are quite different from that of gas flow in conventional reservoirs [42–45]. The percolation mechanism includes diffusion, adsorption/-desorption, and slip flow [46–48].

2.2. Adsorption Models of Shale Gas. The physical adsorption defined by Brunauer et al. [49] occurs when gas contacts a solid surface: some gas molecules are captured by the solid because of the intermolecular force. This means that if the volume of gas is constant, gas pressure drops; if the pressure is constant, the volume of gas decreases. The gas molecules captured by the solid are said to be adsorbed, and the solid is called an adsorbent.

Because shale gas adsorption models are numerous, it is necessary to choose the best one before using it. Here, we use a nonlinear fitting method to analyze the degree of fit between adsorption models and some adsorption data from subcritical and supercritical states.

In the original state of a shale gas reservoir, adsorbed and desorbed gasses are in dynamic pressure equilibrium. When the equilibrium is disturbed after production, the gas adsorbed in the organic matter surfaces begins to desorb, and then the desorbed gas becomes free and is stored in the

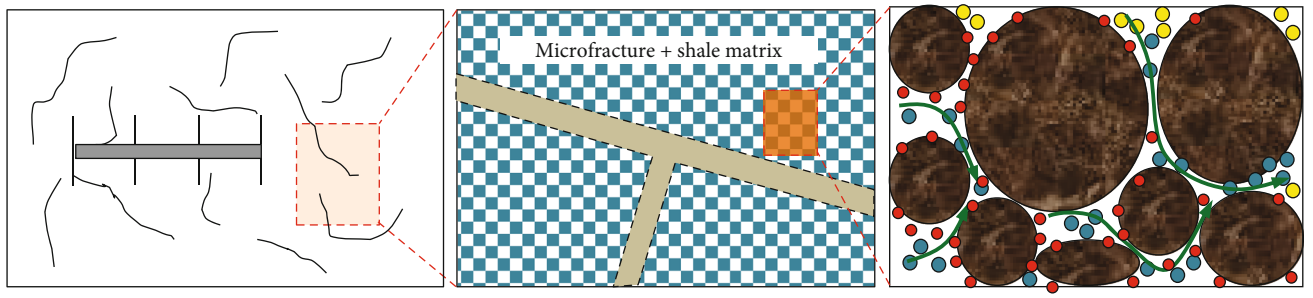

Figure 2: Physical model of pseudosteady flow when gas desorbs from the matrix and diffuses to a fracture [39, 50].

reservoir until the adsorbed and free gasses are in equilibrium again.

Congruent with the previous analysis, the Langmuir isotherm is one of the most popular models used to describe the gas adsorption/desorption process. The amount of gas adsorbed by a solid surface is given by the Langmuir equation below, characterizing the desorption processes as a function of pressure at constant temperature [33]:

$$V = V_L \frac{p_m}{p_L + p_m}, \tag{1}$$

where V is the volume of the adsorbed gas (cm^3/g), P_m is the gas pressure (MPa), V_L is the Langmuir volume (cm^3/g), P_L is the Langmuir pressure (1/MPa).

In addition, the expression of desorbed gas mass flux that desorbs from a reservoir whose volume is V_b during a unit of time is

$$q_{des} = \rho_{gsc} V_b \frac{\partial V}{\partial t}, \tag{2}$$

where q_{des} is the mass flow rate of gas desorption from the reservoir of volume V_b (kg/s), ρ_{gsc} is the density of shale gas under standard conditions (kg/m^3).

Incorporating equation (1) into equation (2) results in

$$q_{des} = \rho_{gsc} V_b V_L \frac{p_L}{(p_m + p_L)^2} \frac{\partial p_m}{\partial t}. \tag{3}$$

Introducing pseudopressure into equation (3), it can be rewritten as [50]

$$q_{des} = \rho_{gsc} V_b V_L \frac{m(p_L)}{(m(p_m) + m(p_L))^2} \frac{\partial m(p_m)}{\partial t}. \tag{4}$$

It is assumed that the desorbed process of shale gas is instantaneous and all the desorbed gas will become free gas, so equation (4) can be used as a continuity equation of a fracture network or matrix.

3. Model for Gas Flow in a Fractured Shale Gas Reservoir

3.1. Physical Model. Macropores exist in a practical shale matrix, which may lead to an error if gas storage and flow are ignored in these macropores. Therefore, researchers have devised a "tri-pore" conceptual model, where the shale gas reservoir consists of matrix pores, macropores, and microfractures. When the adsorbed gas desorbs from the surface of the matrix particles, it enters the macropores first and then flows into the microfractures [39, 50–52]. Figure 2 shows the physical model.

Song [39] first proposed a physical model concerning transfusion in the macropores of the matrix. But it was only a physical seepage-mechanism model, which was not modeled mathematically. In this paper, a mathematical model for this physical conception is proposed and solved. The interporosity flow of free gas between macropores and microfractures can be divided into 2 types: (1) a pseudosteady interporosity flow model and (2) a transient interporosity flow model.

3.2. Comprehensive Mathematical Model

3.2.1. Transient Interporosity Flow Model. When the gas flow from macropores to a fracture network is transient interporosity, the continuity equation in the fracture network is [53, 54]

$$\frac{1}{r^2}\frac{\partial}{\partial r}\left(\frac{k_f}{\mu_g}\rho_g r^2 \frac{\partial p_f}{\partial r}\right) = \frac{\partial\left(\phi_f \rho_g\right)}{\partial t} - q_m. \tag{5}$$

For unsteady interporosity and spherical matrix particles, the continuity equation in the matrix can be expressed as follows:

$$\frac{1}{r_m^2}\frac{\partial}{\partial r_m}\left(\frac{k_m}{\mu_g}\rho_g r_m^2 \frac{\partial p_m}{\partial r_m}\right) = \frac{\partial\left(\phi_m \rho_g\right)}{\partial t} + q_{des}. \tag{6}$$

Because the initial pressure is equal throughout the reservoir, the initial condition in the matrix equals to the initial reservoir pressure p_i:

$$p_m(t=0, r_m) = p_i. \tag{7}$$

Because seepage of the gas in the macropores is symmetrical, the inner boundary condition is

$$\frac{\partial p_m}{\partial r_m}(t, r_m = 0) = 0. \tag{8}$$

Because the outer boundary of the spherical matrix particles is connected to the fracture system, the outer boundary pressure of the matrix is equal to the pressure of the fracture system:

$$p_m(t, r_m = R_m) = p_f. \tag{9}$$

When the flow between the macropores and the microfractures is unsteady, the interporosity flow rate is

$$q_m = -\frac{3\rho_{gm}}{R_m}\frac{k_m}{\mu_g}\frac{\partial p_m}{\partial r_m}\bigg|_{r_m = R_m}. \tag{10}$$

By the Langmuir isotherm equation, the desorption rate of shale gas q_{des} can be written as

$$q_{des} = \rho_g(1-\phi_f-\phi_m)\frac{V_L m(p_L)}{[m(p_L)+m(p_m)]^2}\frac{\partial m(p_m)}{\partial t}. \tag{11}$$

By introducing dimensionless variables into the above mathematical models and then reformatting them by several simple transformations (a detailed derivation process is described in Appendix A, while the dimensionless variables are shown in Appendix B), the dimensionless seepage equation of the fracture system can be obtained as

$$\frac{1}{r_D^2}\frac{\partial}{\partial r_D}\left(r_D^2\frac{\partial \Delta\bar{m}_f}{\partial r_D}\right) = f(s)\Delta\bar{m}_f, \tag{12}$$

where the expression of $f(s)$ is

$$f(s) = \omega_f s + \frac{\lambda}{5}\left[\sqrt{\frac{15(1-\omega_f+\omega_d)s}{\lambda}}\coth\sqrt{\frac{15(1-\omega_f+\omega_d)s}{\lambda}} - 1\right]. \tag{13}$$

3.2.2. Pseudosteady Interporosity Flow Model. For pseudosteady gas flow from the macropores to the fractures, incorporating pseudosteady interporosity flow rate and pseudopressure into the seepage equation of the fracture system, the seepage equation of fracture system can be written as

$$\frac{1}{r}\frac{\partial}{\partial r}\left(r^2\frac{\partial m_f}{\partial r}\right) = \frac{\phi_f\mu_f c_{fgi}}{k_f}\frac{\partial m_f}{\partial t} - \frac{\alpha k_m}{k_t}[m_m - m_f]. \tag{14}$$

For pseudosteady gas flow from the matrix to the fractures, the seepage equation of the macropores is

$$-\alpha\frac{k_m}{k_f}[m_m - m_f] = \frac{\phi_m\mu_{gi}c_{mgi}}{k_f}\frac{\partial m_m}{\partial t} + \frac{\phi_m\mu_{gi}c_d}{k_f}\frac{\partial m_m}{\partial t}, \tag{15}$$

where c_d is an additional compressibility that considers the effect of desorption. The expression of c_d is

$$c_d = \frac{2Tp_{sc}}{\phi_m\mu_{gi}T_{sc}}\frac{(1-\phi_f-\phi_m)V_L m(p_L)}{[m(p_L)+m(p_m)]^2}. \tag{16}$$

Incorporating the above dimensionless variables into the seepage equation of the matrix and the fracture system, the dimensionless seepage equations of the matrix and the fracture system are

$$\frac{1}{r_D}\frac{\partial}{\partial r_D}\left(r_D^2\frac{\partial \Delta m_f}{\partial r_D}\right) = \omega_f\frac{\partial \Delta m_f}{\partial t_D} - \lambda[\Delta m_m - \Delta m_f], \tag{17}$$

$$-\lambda[\Delta m_m - \Delta m_f] = (1-\omega_f)\frac{\partial \Delta m_m}{\partial t_D} + \omega_d\frac{\partial \Delta m_m}{\partial t_D}. \tag{18}$$

Using the Laplace transform method, equations (17) and (18) can be rewritten as

$$\frac{1}{r_D}\frac{\partial}{\partial r_D}\left(r_D^2\frac{\partial \Delta\bar{m}_f}{\partial r_D}\right) = \omega_f s\Delta\bar{m}_f - \lambda[\Delta\bar{m}_m - \Delta\bar{m}_f]s, \tag{19}$$

$$-\lambda[\Delta\bar{m}_m - \Delta\bar{m}_f] = (1-\omega_f+\omega_d)s\Delta\bar{m}_m. \tag{20}$$

According to equations (19) and (20), the seepage equation of the fracture system is

$$\frac{1}{r_D^2}\frac{\partial}{\partial r_D}\left(r_D^2\frac{\partial \Delta\bar{m}_f}{\partial r_D}\right) = f(s)\Delta\bar{m}_f, \tag{21}$$

where

$$f(s) = \frac{\lambda(1+\omega_d)+\omega_f(1-\omega_f+\omega_d)s}{\lambda+(1-\omega_f+\omega_d)s}s. \tag{22}$$

4. MFHWs in a Rectangular Composite Shale Gas Reservoir with an SRV

4.1. Physical Model. In a shale gas or tight-gas reservoir, hydraulic fracturing is widely used to improve the productivity of the reservoir. A MFHW can make the cracks contact the matrix completely, form flow channels, and ensure efficient extraction from an unconventional reservoir [52, 55–58].

In 2008, Mayerhofer et al. [57] studied the change of cracks in Barnett shale by microseismic technology and proposed the SRV concept. The SRV refers to an effective reservoir that is made by hydraulic fracturing, with a composite

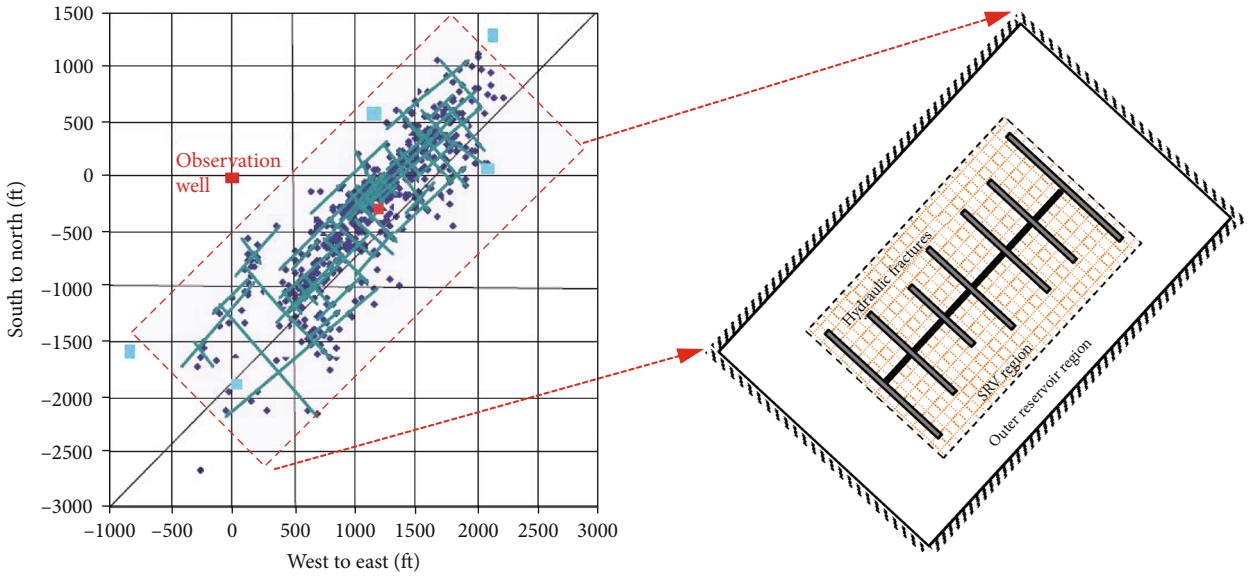

Figure 3: Physical model schematic of fractured wells considering SRV [56].

fracture network formed as a consequence. SRV can maximize the contact surface between matrix and fractures so that the seepage distance of oil and gas in any direction from matrix to cracks will be shortened, which improves the effective permeability of the entire reservoir. According to the microseismic monitoring map for an MFHW in Barnett shale reported by Fisher et al. [56], the physical model (Figure 3: left) can be approximated by the rectangular composite shale gas reservoir conceptual model (Figure 3: right) with enough accuracy, which is better than the circular composite conceptual model for long horizontal well cases.

To simplify the analysis, we use the following basic assumptions for this model: the MFHW is located at the center of a closed rectangular reservoir; the reservoir length, width, and height are x_e, y_e, and h, respectively; the fractures are perpendicular to the horizontal well and randomly distributed along it; the effective well length is L (from the leftmost to the rightmost fractures); each fracture is symmetrical or asymmetrical, and the fracture half-lengths are L_{fui} and L_{fli}; the length and width of the SRV region are x_m and y_m, respectively; the number of fractures is M, and every fracture has infinite conductivity; no flow from the matrix to the wellbore and the pressure drop caused by the gas flow through the wellbore are ignored.

4.2. Boundary Element Model of a Composite Rectangular Gas Reservoir considering the SRV. According to the physical model described above, the governing equation for gas flow in an inner fracture network system is ([59–62], 2019)

$$\frac{\partial \Delta \bar{m}_{f1}}{\partial x_D^2} + \frac{\partial \Delta \bar{m}_{f1}}{\partial y_D^2} + \frac{\partial \Delta \bar{m}_{f1}}{\partial z_D^2} + \frac{2Tp_{sc}}{k_{f1}T_{sc}h}\frac{q_{v1}}{s}\delta \cdot \left(x_D - x'_{s1D}x, y_D - y'_{s1D}, z_D - z'_{s1D}\right) = f_1(s)\Delta \bar{m}_{f1}. \tag{23}$$

For the outer region

$$\frac{\partial \Delta \bar{m}_{f2}}{\partial x_D^2} + \frac{\partial \Delta \bar{m}_{f2}}{\partial y_D^2} + \frac{\partial \Delta \bar{m}_{f2}}{\partial z_D^2} + \frac{2Tp_{sc}}{k_{f2}T_{sc}h}\frac{q_{v2}}{s}\delta \cdot \left(x_D - x'_{s1D}, y_D - y'_{s1D}, z_D - z'_{s1D}\right) = f_2(s)\Delta \bar{m}_{f2}. \tag{24}$$

The cohesive conditions on the surface between the inner and outer regions are

$$\begin{aligned} \Delta \bar{m}_{f1} &= \Delta \bar{m}_{f2}, \quad (x_D, y_D, z_D) \in S_{interface}, \\ \frac{\partial \Delta \bar{m}_{f1}}{\partial n_D} &= -\frac{1}{M_{12}}\frac{\partial \Delta \bar{m}_{f2}}{\partial n_D}, \quad (x_D, y_D, z_D) \in S_{interface}. \end{aligned} \tag{25}$$

Because the outer boundary of our model is closed, the outer boundary condition is

$$\frac{\partial \Delta \bar{m}_{f2}}{\partial n} = 0, \quad (x_D, y_D, z_D) \in S_{interface}. \tag{26}$$

Incorporating the dimensionless variables defined in Appendix B into equations (23) and (24), the mathematical model in the Laplace space becomes

$$\frac{\partial \Delta m_{f1D}}{\partial x_D^2} + \frac{\partial \Delta m_{f1D}}{\partial y_D^2} + \frac{\partial \Delta m_{f1D}}{\partial z_D^2} = f_1(s)\Delta \bar{m}_{f1D} - \frac{2\pi q_{v1D}}{sM_{12}}\delta\left(x_D - x'_{s1D}, y_D - y'_{s1D}, z_D - z'_{s1D}\right), \tag{27}$$

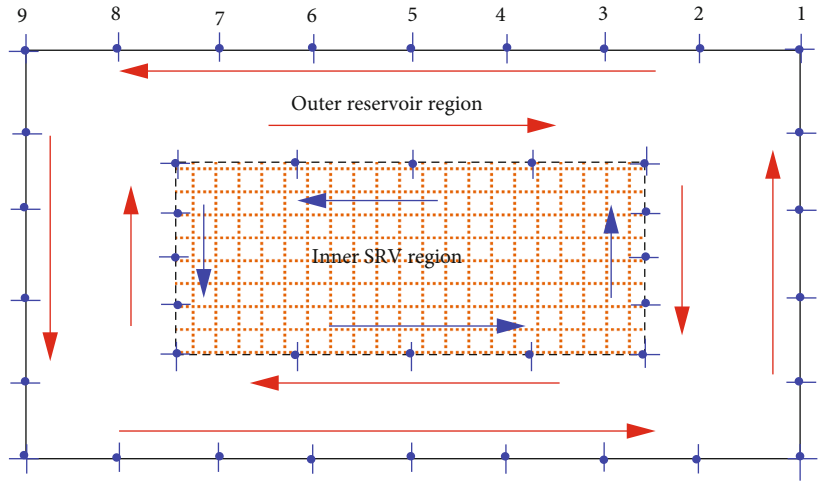

Figure 4: Grid of the inner and outer boundaries and the sequence of the discrete elements in a rectangular composite gas reservoir.

$$\frac{\partial \Delta m_{f2D}}{\partial x_D^2} + \frac{\partial \Delta m_{f2D}}{\partial y_D^2} + \frac{\partial \Delta m_{f2D}}{\partial z_D^2} = f_2(s)\Delta \bar{m}_{f2D} - \frac{2\pi q_{v2D}}{s}\delta\left(x_D - x'_{s1D}, y_D - y'_{s1D}, z_D - z'_{s1D}\right), \tag{28}$$

$$m_{f1D} = m_{f2D}, \quad (x_D, y_D, z_D) \in S_{interface}, \tag{29}$$

$$\frac{\partial m_{f1D}}{\partial n_D} = -\frac{1}{M_{12}}\frac{\partial m_{f2D}}{\partial n_D}, \quad (x_D, y_D, z_D) \in S_{interface}. \tag{30}$$

When using the boundary element method to solve the model above, the fundamental solutions of differential equations are needed. It is assumed that the fundamental solutions of the inner and outer regions in the shale gas reservoir are $E_1(R_D, R'_D, s)$ and $E_2(R_D, R'_D, s)$, respectively, which satisfy

$$\nabla^2 E_1\left(R_D, R'_D, s\right) - f_1(s)E_1\left(R_D, R'_D, s\right) + 2\pi\delta\left(R_D, R'_D\right) = 0, \tag{31}$$

$$\nabla^2 E_2\left(R_D, R'_D, s\right) - f_2(s)E_1\left(R_D, R'_D, s\right) + 2\pi\delta\left(R_D, R'_D\right) = 0. \tag{32}$$

Since the fractures are assumed completely open in this paper, the expressions of fundamental solutions E_1 and E_2 are

$$E_1 = K_0\left[\sqrt{f_1(s)}\left(R_D - R'_D\right)\right], \quad E_2 = K_0\left[\sqrt{f_2(s)}\left(R_D - R'_D\right)\right]. \tag{33}$$

Both sides of equations (31) and (32) are multiplied by m_{f1D} and m_{f2D}, respectively, and the equations can be obtained by

$$m_{f1D}\nabla^2 E_1 - f_1(s)m_{f1D}E_1 + 2\pi m_{f1D}\delta\left(R_D, R'_D\right) = 0, \tag{34}$$

$$m_{f2D}\nabla^2 E_2 - f_2(s)m_{f2D}E_1 + 2\pi m_{f2D}\delta\left(R_D, R'_D\right) = 0. \tag{35}$$

Both sides of equations (23) and (28) are multiplied by E_1 and E_2, respectively, and we have

$$E_1\nabla^2 m_{f1D} = f_1(s)E_1\Delta \bar{m}_{f1D} - E_1\frac{2\pi q_{v1D}}{sM_{12}}\delta\left(R_D - R'_{wD}\right), \tag{36}$$

$$E_2\nabla^2 m_{f1D} = f_1(s)E_2\Delta \bar{m}_{f1D} - E_2\frac{2\pi q_{v2D}}{s}\delta\left(R_D - R'_{wD}\right). \tag{37}$$

Using equations (34) and (35) minus equations (36) and (37), respectively, the equations can be transformed as

$$m_{f1D}\nabla^2 E_1 - E_1\nabla^2 m_{f1D} + 2\pi m_{f1D}\delta\left(R_D, R'_D\right) = E_1\frac{2\pi q_{v1D}}{sM_{12}}\delta\left(R_D - R'_{wD}\right), \tag{38}$$

$$m_{f2D}\nabla^2 E_2 - E_2\nabla^2 m_{f2D} + 2\pi m_{f2D}\delta\left(R_D, R'_D\right) = E_2\frac{2\pi q_{v2D}}{s}\delta\left(R_D - R'_{wD}\right). \tag{39}$$

Integrating equations (38) and (39) on the inner region Ω_1 and outer region Ω_2, respectively, we have

$$\int_{\Omega_1}\left[m_{f1D}\nabla^2 E_1 - E_1\nabla^2 m_{f1D} + 2\pi m_{f1D}\delta\left(R_D, R'_D\right) - E_1\frac{2\pi q_{v1D}}{sM_{12}} \cdot \delta\left(R_D - R'_{wD}\right)\right]d\Omega_1 = 0, \tag{40}$$

Table 2: Reservoir properties.

Reservoir property	Value	Reservoir property	Value
Permeability of SRV, k_{f1} (mD)	0.05	Porosity of SRV, $\varnothing_{f1}$ (fraction)	0.05
Permeability of outer reservoir, k_{f2} (mD)	0.01	Porosity of SRV, $\varnothing_{f2}$ (fraction)	0.002
Length of SRV, x_m (m)	1600	Width of SRV, y_m (m)	400
Inner matrix permeability, k_{m1} (mD)	0.0001	Inner matrix porosity, $\varnothing_{m1}$	0.01
Outer matrix permeability, k_{m2} (mD)	0.0001	Outer matrix porosity, $\varnothing_{m2}$	0.01
Wellbore storage coefficient, C_D (dimensionless)	1×10^{-4}	Gas relative density, γ_g (fraction)	0.65

$$\int_{\Omega_2}\left[m_{f2D}\nabla^2 E_2 - E_2\nabla^2 m_{f2D} + 2\pi m_{f2D}\delta\left(R_D, R_D'\right) - E_2\frac{2\pi q_{v2D}}{s} \cdot \delta\left(R_D - R_{wD}'\right)\right]d\Omega_2 = 0. \tag{41}$$

We use Green's second identity as follows [61, 62]:

$$\int_{\Omega}\left(\mu\nabla^2\nu - \nu\nabla^2\mu\right)d\Omega' = \int_s(\mu\nabla\nu - \nu\nabla\mu)dS', \tag{42}$$

where $S(S = \sum_i S_i)$ is the entire boundary of region Ω.

Based on the characteristics of equation (42) and the delta function, the differential equation of the inner and outer regions can be changed into an integral equation on the boundary, and the boundary integral equations of equations (40) and (41) are

$$m_{f1D}(R_D) = \frac{1}{2\pi}\int_{S_1}[E_1\nabla m_{f1D} - m_{f1D}\nabla E_1]dS_1' + \frac{1}{M_{12}s}\int_{\Omega_1} q_{v1D}\left(R_{s1D}'\right)E_1 d\Omega_1', \tag{43}$$

$$m_{f2D}(R_D) = \frac{1}{2\pi}\int_{S_2}[E_2\nabla m_{f2D} - m_{f2D}\nabla E_2]dS_2' + \frac{1}{s}\int_{\Omega_2} q_{v2D}\left(R_{s2D}'\right)E_2 d\Omega_2'. \tag{44}$$

There are two kind of boundaries (the outer and the inner) in the gas reservoir. It is assumed that the outer boundary can be discretized into NO elements and the inner boundary can be discretized into NI elements, so the total number of the elements for the boundaries is NO + NI. The serial number of inner boundary elements is clockwise, while it is counterclockwise for outer boundary elements, as shown in Figure 4.

For the integral equation on the boundary, R_D is an arbitrary point on the boundary, while R_D' is an arbitrary point in the reservoir region. R_{S1D} and R_{S2D} are the dimensionless coordinates of source points in the inner and outer regions, respectively. If R_D' is not only in the reservoir region but also on the boundaries, equations (43) and equations (44) can be rewritten as

$$\theta m_{f1D}(R_D) = \frac{1}{2\pi}\int_{S_1}[E_1\nabla m_{f1D} - m_{f1D}\nabla E_1]dS_1' + \frac{1}{M_{12}s}\int_{\Omega_1} q_{v1D}\left(R_{s1D}'\right)E_1 d\Omega_1', \tag{45}$$

$$\theta m_{f2D}(R_D) = \frac{1}{2\pi}\int_{S_2}[E_2\nabla m_{f2D} - m_{f2D}\nabla E_2]dS_2' + \frac{1}{s}\int_{\Omega_2} q_{v2D}\left(R_{s2D}'\right)E_2 d\Omega_2', \tag{46}$$

where θ is a constant related to the geometric shape of R_D', and the expression of θ is [62]

$$\theta = \frac{\alpha}{2\pi}, \tag{47}$$

where α is the angle of the boundary tangent line at R_D'.

Incorporating the fundamental solutions E_1 and E_2 into equations (45) and (46), a series of linear equation sets can be obtained by solving the reservoir points R_D' along the boundary points and fracture points, after which the dimensionless pseudopressure response curves of the fractured well can be obtained by solving the equation sets above. Due to the complexity of the process, its details are not shown in this article; interested readers may consult these papers for details: [52, 59, 60, 63–71].

4.3. Pressure and Production Type Curve Analysis. The boundary element method is employed to acquire type curves of dimensionless bottomhole pressures at constant rate, and the production rate and cumulative production at a constant pressure are based on the parameters in Table 2.

Figure 5 shows the well-test type curves of reservoirs with different sizes and SRVs. The following flow stages can be observed when the reservoir and SRV sizes are large enough:

(a) Stage 1: early wellbore storage

(b) Stage 2: transition flow between wellbore storage and early linear flow of a fracture system. A hump is in the pseudopressure derivative curve for this stage,

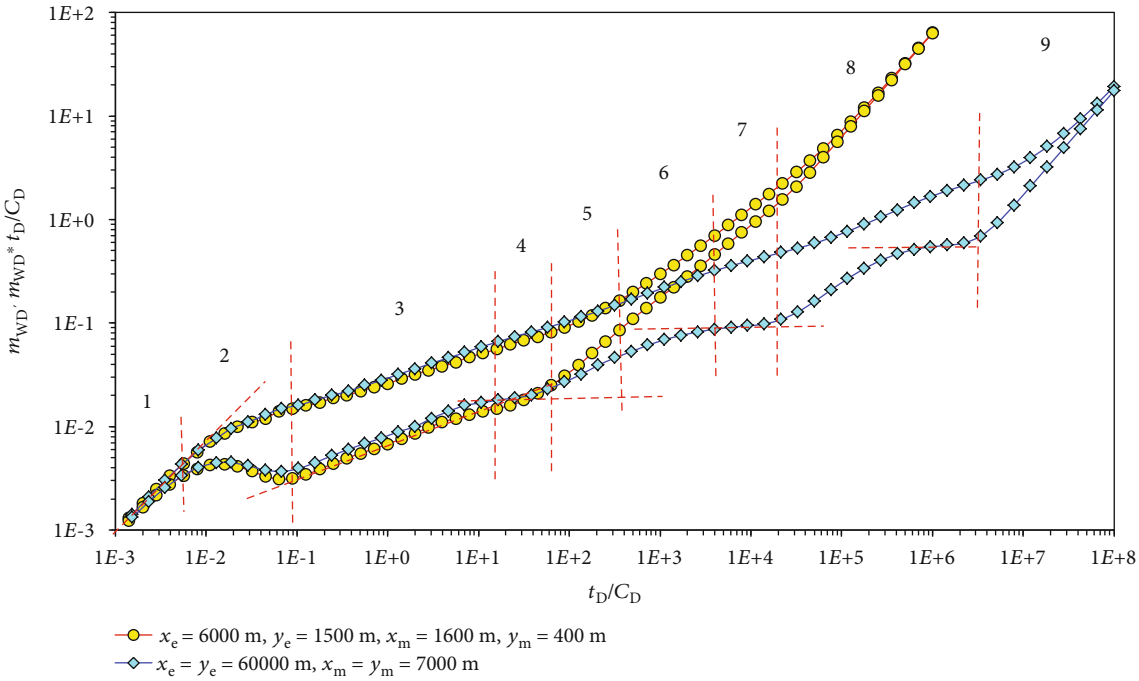

Figure 5: Effect of reservoir size on type curves.

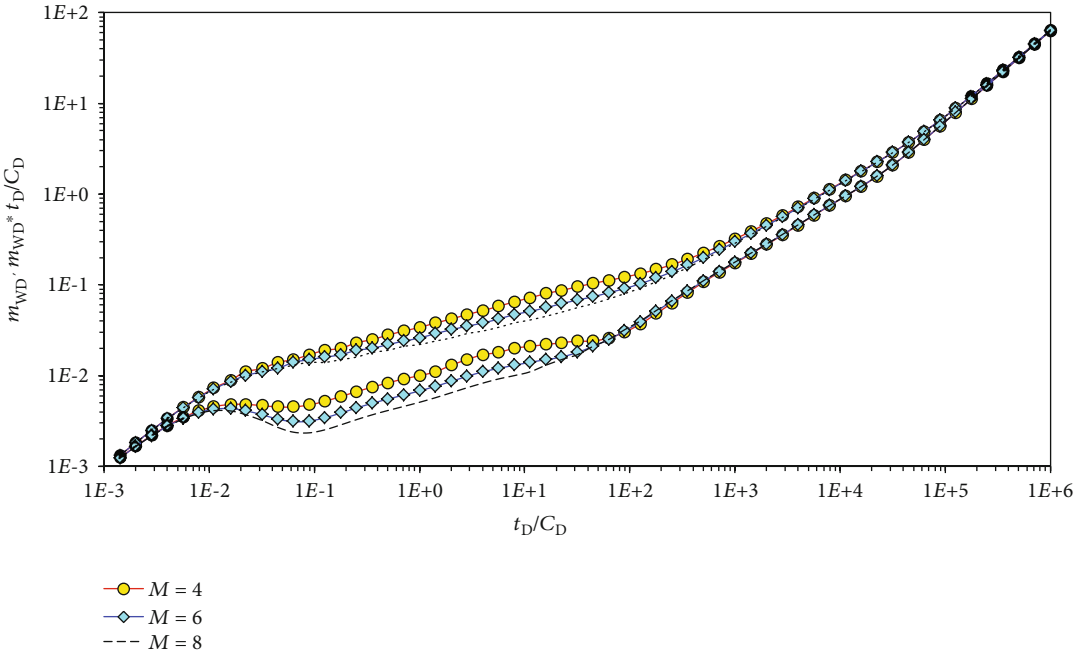

Figure 6: Effect of fractures number on well-test type curves.

and the height and width of the hump depend on the wellbore storage and skin factor

(c) Stage 3: early linear flow of the fracture system. In this flow stage, the pseudopressure derivative curve is a straight line, and the slope is 0.5. The position of the straight line is controlled by the permeability of the SRV, and the length of this straight line is related to the permeability of the SRV, the fracture length, and the distance between the fractures

(d) Stage 4: early radial flow of fracture system. For this stage, the pseudopressure derivative curve is a portion of a horizontal straight line. In addition, when the height of the SRV is close to the length

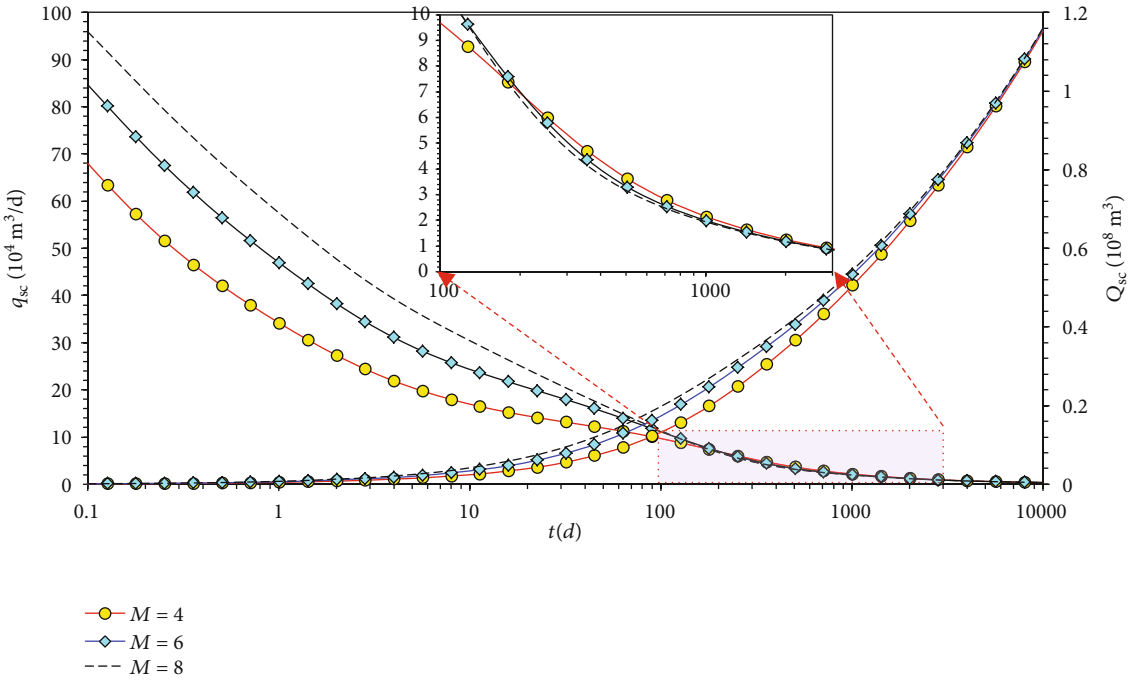

Figure 7: Effects of number of fractures on production rate and cumulative production curves.

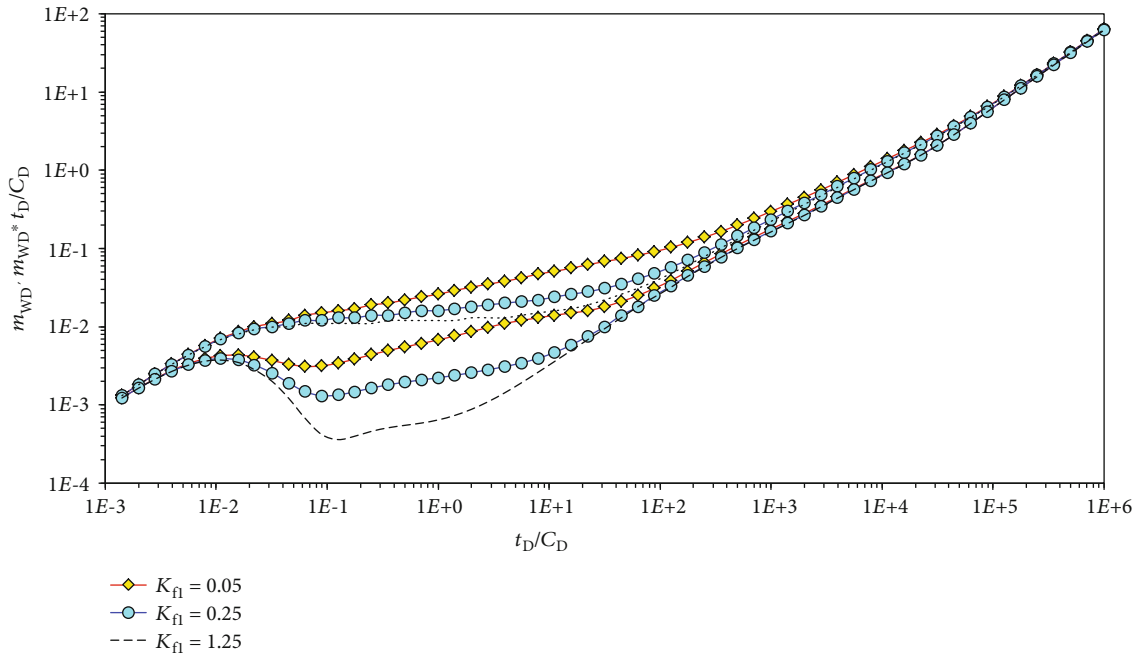

Figure 8: Effect of SRV permeability on well-test type curves.

of the fracture, this line may be covered or offset under the effect of outer reservoir properties

(e) Stage 5: transition flow between early radial flow of the fracture system and radial flow of the SRV

(f) Stage 6: radial flow of the SRV. For this stage, the pseudopressure derivative curve is a section of a horizontal straight line. It is found that the higher the permeability of the SRV, the lower the position of this horizontal line

(g) Stage 7: transition flow between radial flow of the SRV and radial flow of the outer region

(h) Stage 8: radial flow of the outer region. In this stage, the pseudopressure derivative curve is a straight line whose slope is 0.5

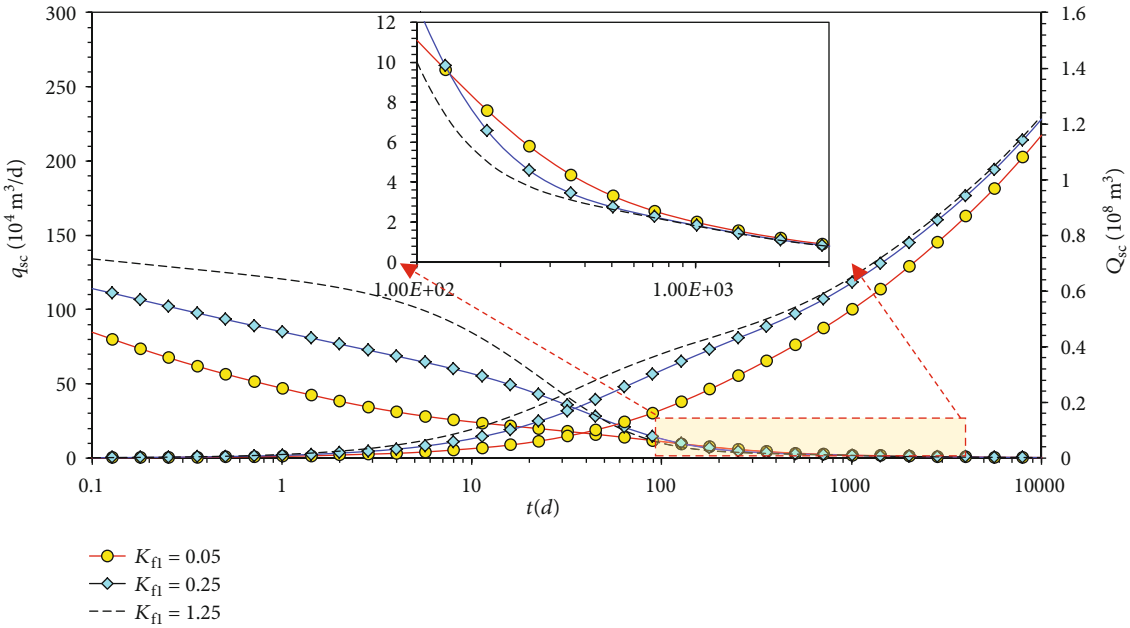

Figure 9: Effects of SRV permeability on production rate and cumulative production curves.

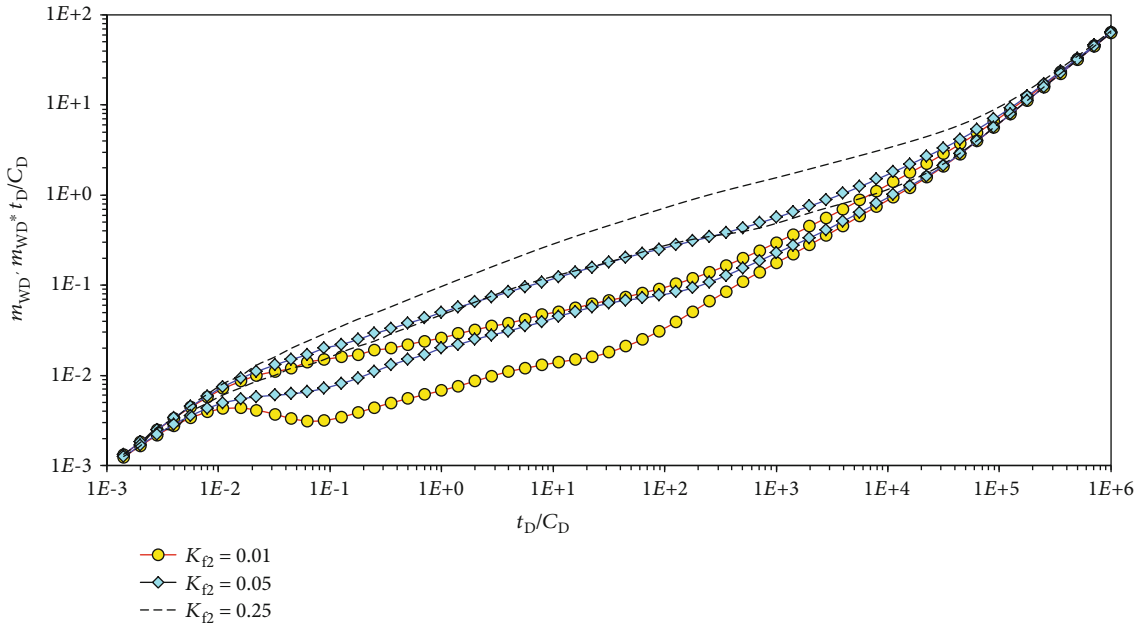

Figure 10: Effect of reservoir permeability on well-test type curves.

(i) Stage 9: boundary-dominated flow. For this stage, the pseudopressure and pseudopressure derivative curves overlap, and this section is a straight line with a slope of 1. Because $x_e = y_e = 60000$ m, there is no linear flow of the reservoir

When the sizes of the reservoir and the SRV are reasonable, the pseudopressure and pseudopressure derivative curves are shown in Figures 5–11 as the plots with yellow pellets. After the early linear flow of the fracture system, the pressure reaches the region close to the reservoir boundary, so the curves turn upward, and then the pseudopressure and pseudopressure derivative curves are almost parallel to each other as a straight line, but the slope is not 0.5. When the pressure reaches the reservoir boundary, the 2 curves overlap.

Figures 6 and 7 show the effects of the fracture number on well-test type curves (dimensionless pseudopressure and its derivative) and production curves (production rate and cumulative production), respectively. As shown in Figure 6, for a constant reservoir size and SRV, the number of hydraulic fractures affects mainly the early flow periods following

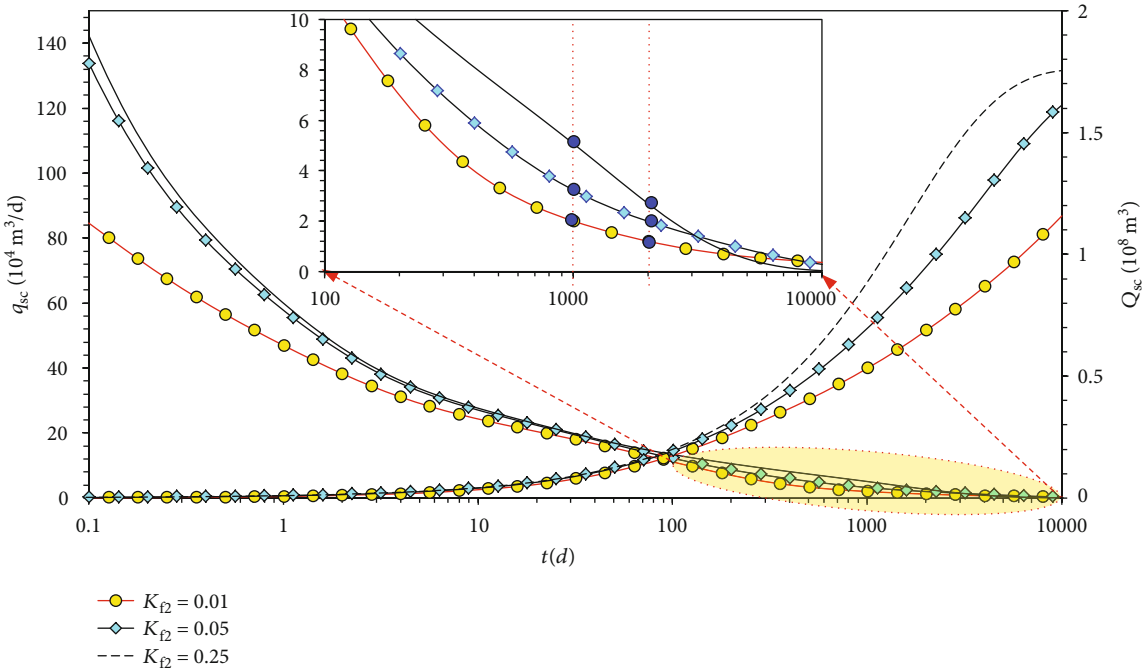

Figure 11: Effects of reservoir permeability on production rate and cumulative production curves.

Table 3: Well production rates for different reservoir permeabilities at different times.

Reservoir permeability (mD)	Production rate (10^4 m^3/d)	
	1000 (d)	2000 (d)
0.25	5.42	2.78
0.05	3.41	2.01
0.01	1.99	1.19

the wellbore storage flow period. When the pressure wave transports to the outer region, the effects will vanish and all pressure and pressure derivative curves will coincide. When a well produces at a constant rate, the higher the fracture number, the higher the early production; this effect lasts for just a few years.

Figures 8 and 9 show the effects of different flow region permeabilities on well-test type curves and production curves, respectively. The effects occur in the middle flow stage. The position of the well-test type curves is lower when the SRV permeability is higher, but the difference between the well-test type curves becomes smaller and smaller as the pressure reaches the reservoir boundary. Figure 9 shows that when SRV permeability increases, the early production rate is higher than the previous one, the production rate is much higher in the middle stage, and the SRV permeability has no effect on the final cumulative production.

Figures 10 and 11 show the effects of reservoir permeability on type curves and production curves, respectively. Because the reference permeability in our model is the reservoir permeability, the reservoir permeability has the opposite effect on type curves compared to that of SRV. The higher the reservoir permeability, the higher the location of the type curves (as shown in Figure 10), which does not mean that the drawdown pressure is higher. When the well is producing at constant pressure, the gas supply is timely due to the high permeability of the reservoir, and gas production rate increases with reservoir permeability increasing (as shown in Figure 11). Even in the later production period when the well has been producing for 1000 d and 2000 d, the well production rate for a reservoir with a higher permeability is still much higher, as shown in Table 3. Therefore, a desert area is very important for the exploitation and development of unconventional shale gas reservoirs.

5. Conclusions

We established a comprehensive mathematical model to describe a multistage fractured horizontal well in a rectangular composite shale gas reservoir with an SRV, and the solution was also obtained by a boundary element method. The main conclusions we derived are as follows:

(1) A composite rectangular model of a fractured horizontal well using the "tri-pores" conceptual model is proposed in this paper, and the complex model was solved by BEM, which has not been comprehensively reported before

(2) The number of fractures affects the well production rate at primarily the early flow period; the effect on the later flow period is weak

(3) The permeability in the SRV region has a substantial effect on the early well production rate; the higher the permeability, the greater the rate will be

(4) During the intermediate flow period, the effect will be the opposite, which can be explained by mass conservation for a closed constant-volume gas reservoir

Appendix

A. Transformations

Let $m_f = m(p_f)$ and $m_m = m(p_m)$; then the pseudopressure and gas density expression are introduced into equation (5), so the continuity equation in the fracture network is

$$\frac{1}{r^2}\frac{\partial}{\partial r}\left(r^2\frac{\partial m_f}{\partial r}\right) = \frac{\mu_{gi}\phi_f c_{fgi}}{k_f}\frac{\partial m_f}{\partial t} + \frac{3}{R_m}\frac{k_m}{k_f}\frac{\partial m_m}{\partial r_m}\bigg|_{r_m=R_m}. \quad (A.1)$$

The shape factor of the spherical matrix particles is

$$\alpha = \frac{15}{R_m^2}. \quad (A.2)$$

Inserting the shape factor into equation (A.1) yields

$$\frac{1}{r^2}\frac{\partial}{\partial r}\left(r^2\frac{\partial m_f}{\partial r}\right) = \frac{\mu_{gi}\phi_f c_{fgi}}{k_f}\frac{\partial m_f}{\partial t} + \frac{\alpha R_m}{5}\frac{k_m}{k_f}\frac{\partial m_m}{\partial r_m}\bigg|_{r_m=R_m}. \quad (A.3)$$

Inserting equation (11) into equation (6) yields

$$\frac{1}{r_m^2}\frac{\partial}{\partial r_m}\left(\frac{k_m}{\mu_g}\rho_g {r_m}^2\frac{\partial p_m}{\partial r_m}\right) = \frac{\phi_m\mu_{gi}c_{mgi}}{k_m}\frac{\partial m_m}{\partial t} + \frac{\phi_m\mu_{gi}c_d}{k_m}\frac{\partial m_m}{\partial t}, \quad (A.4)$$

where c_d is an additional compressibility taking into account the effect of desorption; the expression is given in the following formula:

$$c_d = \frac{2Tp_{sc}}{\phi_m\mu_{gi}T_{sc}}\frac{(1-\phi_f-\phi_m)V_L m(p_L)}{[m(p_L)+m(p_m)]^2}. \quad (A.5)$$

The initial condition of the spherical matrix is

$$m_m|(t=0, r_m) = m(p_i). \quad (A.6)$$

The inner boundary condition of the spherical matrix is

$$\frac{\partial m_m}{\partial r_m}\bigg|(t, r_m = 0) = 0. \quad (A.7)$$

The outer boundary condition of the matrix is

$$m_m|(t, r_m = R_m) = m_f. \quad (A.8)$$

All the dimensionless variables are defined as

$$\begin{aligned}
r_{mD} &= \frac{r_m}{R_m},\\
r_D &= \frac{r}{L_{ref}},\\
t_D &= \frac{k_f t}{(\phi_m c_{mgi} + \phi_f c_{fgi})\mu_{gi}L_{ref}^2},\\
\omega_f &= \frac{\phi_f c_{fgi}}{\phi_m c_{mgi} + \phi_f c_{fgi}},\\
\omega_d &= \frac{\phi_m c_d}{\phi_m c_{mgi} + \phi_f c_{fgi}},\\
\lambda &= \alpha\frac{k_m}{k_f}L_{ref}^2,\\
\Delta m_f &= m(p_i) - m(p_f),\\
\Delta m_m &= m(p_i) - m(p_m).
\end{aligned} \quad (A.9)$$

Inserting the dimensionless variables above into the seepage model of the matrix and fracture network, we can rewrite the model as

$$\begin{aligned}
&\frac{1}{r_D^2}\frac{\partial}{\partial r_D}\left(r_D^2\frac{\partial \Delta m_f}{\partial r_D}\right) = \omega_f\frac{\partial \Delta m_f}{\partial t_D} + \frac{\lambda}{5}\frac{\partial \Delta m_m}{\partial r_{mD}}\bigg|_{r_{mD}=1},\\
&\frac{1}{r_{mD}^2}\frac{\partial}{\partial r_{mD}}\left(r_{mD}^2\frac{\partial \Delta m_m}{\partial r_{mD}}\right) = \frac{15(1-\omega_f)}{\lambda}\frac{\partial \Delta m_m}{\partial t_D} + \frac{15\omega_d}{\lambda}\frac{\partial \Delta m_m}{\partial t_D},\\
&\Delta m_m|(t_D = 0, r_{mD}) = 0,\\
&\frac{\partial \Delta m_m}{\partial r_{mD}}\bigg|(t_D, r_{mD} = 0) = 0,\\
&\Delta m_m|(t_D, r_{mD} = 1) = \Delta m_f.
\end{aligned} \quad (A.10)$$

Using the Laplace transform method, we can get

$$\Delta\bar{m} = \int_0^\infty \Delta m e^{-st_D}\mathrm{d}t_D. \quad (A.11)$$

And the model above can be written as

$$\frac{1}{r_D^2}\frac{\partial}{\partial r_D}\left(r_D^2\frac{\partial \Delta\bar{m}_f}{\partial r_D}\right) = \omega_f s\Delta\bar{m}_f + \frac{\lambda}{5}\frac{\partial \Delta\bar{m}_m}{\partial r_{mD}}\bigg|_{r_{mD}=1}, \quad (A.12)$$

$$\frac{1}{r_{mD}^2}\frac{\partial}{\partial r_{mD}}\left(r_{mD}^2\frac{\partial \Delta\bar{m}_m}{\partial r_{mD}}\right) = \frac{15s(1-\omega_f+\omega_d)}{\lambda}\Delta\bar{m}_m, \quad (A.13)$$

$$\Delta\bar{m}_m|(t_D = 0, r_{mD}) = 0, \quad (A.14)$$

$$\frac{\partial \Delta\bar{m}_m}{\partial r_{mD}}\bigg|(t_D, r_{mD} = 0) = 0, \quad (A.15)$$

$$\Delta\bar{m}_m|(t_D, r_{mD} = 1) = \Delta\bar{m}_f. \quad (A.16)$$

Do the following variable substitution

$$W = r_{\mathrm{mD}} \Delta \bar{m}_{\mathrm{m}}. \tag{A.17}$$

Inserting equation (A.17) into equation (A.13), we have

$$\frac{\partial^2 W}{\partial r_{\mathrm{mD}}^2} = \frac{15s(1-\omega_{\mathrm{f}}+\omega_{\mathrm{d}})}{\lambda} W. \tag{A.18}$$

According to the characteristics of the above equation, the general solution of equation (A.18) can be obtained easily by

$$W = A \sinh\left(\sqrt{g} r_{\mathrm{mD}}\right) + B \cosh\left(\sqrt{g} r_{\mathrm{mD}}\right), \tag{A.19}$$

where

$$g = \frac{15(1-\omega_{\mathrm{f}}+\omega_{\mathrm{d}})s}{\lambda}. \tag{A.20}$$

Inserting equation (A.19) into equation (A.17),

$$\Delta \bar{m}_{\mathrm{m}} = \frac{A \sinh\left(\sqrt{g} r_{\mathrm{mD}}\right) + B \cosh\left(\sqrt{g} r_{\mathrm{mD}}\right)}{r_{\mathrm{mD}}}. \tag{A.21}$$

B can be determined by the inner boundary condition, and A can be determined by the outer boundary condition. A and B have the following values:

$$B = 0, \tag{A.22}$$

$A = \Delta \bar{m}_{\mathrm{f}} / \sinh\left(\sqrt{g}\right)$.

Incorporating the value of A and B into equation (A.21) yields

$$\Delta \bar{m}_{\mathrm{m}} = \frac{\Delta \bar{m}_{\mathrm{f}}}{\sinh\left(\sqrt{g}\right)} \frac{\sinh\left(\sqrt{g} r_{\mathrm{mD}}\right)}{r_{\mathrm{mD}}}. \tag{A.23}$$

The derivative of equation (A.23) is

$$\left.\frac{\partial \Delta \bar{m}_{\mathrm{m}}}{\partial r_{\mathrm{mD}}}\right|_{r_{\mathrm{mD}}=1} = \left[\sqrt{g} \coth\left(\sqrt{g}\right) - 1\right] \Delta \bar{m}_{\mathrm{f}}. \tag{A.24}$$

Incorporating equation (A.24) into equation (A.12) and then simplifying it, we can then obtain the following:

$$\frac{1}{r_{\mathrm{D}}^2} \frac{\partial}{\partial r_{\mathrm{D}}} \left(r_{\mathrm{D}}^2 \frac{\partial \Delta \bar{m}_{\mathrm{f}}}{\partial r_{\mathrm{D}}} \right) = f(s) \Delta \bar{m}_{\mathrm{f}}, \tag{A.25}$$

where the expression of $f(s)$ is

$$f(s) = \omega_{\mathrm{f}} s + \frac{\lambda}{5} \left[\sqrt{\frac{15(1-\omega_{\mathrm{f}}+\omega_{\mathrm{d}})s}{\lambda}} \coth \sqrt{\frac{15(1-\omega_{\mathrm{f}}+\omega_{\mathrm{d}})s}{\lambda}} - 1 \right]. \tag{A.26}$$

B. Dimensionless variables

All the dimensionless variables are defined as

$$\begin{aligned}
r_{\mathrm{D}} &= \frac{r}{L_{\mathrm{ref}}}, \\
t_{\mathrm{D}} &= \frac{k_{\mathrm{f}} t}{\left(\phi_{\mathrm{m}} c_{\mathrm{mgi}} + \phi_{\mathrm{f}} c_{\mathrm{cgi}}\right) \mu_{\mathrm{gi}} L_{\mathrm{ref}}^2}, \\
\omega_{\mathrm{f}} &= \frac{\phi_{\mathrm{f}} c_{\mathrm{fgi}}}{\phi_{\mathrm{m}} c_{\mathrm{mgi}} + \phi_{\mathrm{f}} c_{\mathrm{fgi}}}, \\
\omega_{\mathrm{d}} &= \frac{\phi_{\mathrm{m}} c_{\mathrm{d}}}{\phi_{\mathrm{m}} c_{\mathrm{mgi}} + \phi_{\mathrm{f}} c_{\mathrm{fgi}}}, \\
\lambda &= \alpha \frac{k_{\mathrm{m}}}{k_{\mathrm{f}}} L_{\mathrm{ref}}^2, \\
\Delta m_{\mathrm{f}} &= m(p_i) - m(p_{\mathrm{f}}), \\
\Delta m_{\mathrm{m}} &= m(p_i) - m(p_{\mathrm{m}}).
\end{aligned} \tag{B.1}$$

Data Availability

The production data used to support the findings of this study are included within the article.

Conflicts of Interest

The authors declare that they have not conflicts of interests.

Acknowledgments

This work was supported by the Demonstration Project of the National Science and Technology of China (Grant No. 2016ZX05062), the Science and Technology Major Project of PetroChina (Grant No. 2016E-0611), and the National Science and Technology Major Project of the Ministry of Science and Technology of China (Grant No. 2017ZX05037-001)

References

[1] A. G. Adesida, I. Akkutlu, D. E. Resasco, and C. S. Rai, "Characterization of Barnett shale kerogen pore size distribution using DFT analysis and grand canonical Monte Carlo simulations," in *Paper SPE 147397-MS Presented at SPE Annual Technical Conference and Exhibition*, Denver, Colorado, USA, 2011.

[2] C. McGlade, J. Speirs, and S. Sorrell, "Unconventional gas—a review of regional and global resource estimates," *Energy*, vol. 55, pp. 571–584, 2013.

[3] A. Hadkin and R. Bloom, *Energy Information Administration*, 2016, //http://www.eia.gov/dnav/ng/ng_prod_sum_a_EPG0_FGW_mmcf_m.html.

[4] M. E. Curtis and R. J. Ambrose, "Structural characterization of gas shale on the micro- and nano-scales," in *Paper SPE 137693-MS Presented at Canadian Unconventional Resources and International Petroleum Conference*, Calgary, Alberta, Canada, 2010.

[5] C. J. Houghton and R. V. Westermark, "North Sea downhole corrosion: identifying the problem implementing solutions," *Journal of Petroleum Technology*, vol. 35, no. 1, pp. 239–246, 2013.

[6] J. P. Vermylen and M. D. Zoback, "Hydraulic fracturing, micro seismic magnitudes and stress evolution in the Barnett shale," in *Paper SPE 140507-MS Presented at SPE Hydraulic Fracturing Technology Conference*, The Woodlands, Texas, USA, 2011.

[7] F. Kucuk and W. K. Sawyer, "Transient flow in naturally fractured reservoirs and its application to Devonian gas shale," in *Paper SPE 9397-MS Presented at SPE Annual Technical Conference and Exhibition, 21-24 September*, Dallas, Texas, USA, 1980.

[8] D. E. Lancaster and J. M. Gatens III, "Practical well test analysis methods for hydraulically fractured wells in dual-porosity reservoirs," in *Paper SPE 15924-MS Presented at SPE Eastern Regional Meeting, 12-14 November, Columbus*, USA, Ohio, USA, 1986.

[9] J. L. Johnston and W. J. Lee, "Identification of productive layers in low-permeability gas wells," *SPE Journal of Petroleum Technology*, vol. 44, no. 11, pp. 1240–1248, 2013.

[10] M. Brown, E. Ozkan, R. Raghavan, and H. Kazemi, "Practical solutions for pressure transient responses of fractured horizontal wells in unconventional reservoirs," in *Paper SPE 125043-MS Presented at SPE Annual Technical Conference and Exhibition, 4-7 October*, New Orleans, Louisiana, USA, 2009.

[11] E. Ozkan, M. L. Brown, R. Raghavan, and H. Kazemi, "Comparison of fractured-horizontal-well performance in tight sand and shale reservoirs," *SPE Reservoir Evaluation & Engineering*, vol. 14, no. 2, pp. 248–259, 2013.

[12] R. O. Bello and R. A. Watenbargen, "Multi-stage hydraulically fractured horizontal shale gas well rate transient analysis," in *Paper SPE 126754-MS Presented at the North Arica Technical Conference and Exhibition*, Cairo, Egypt, 2010.

[13] H. A. Al-Ahmadi, A. M. Almarzooq, and R. A. Watenbargen, "Application of linear flow analysis to shale gas wells—field cases," in *Paper SPE 130370-MS Presented at the SPE Unconventional Gas Conference*, Pittsburgh, Pennsylvania, USA, 2010.

[14] E. Stalgorova and L. Mattar, "Practical analytical model to simulate production of horizontal wells with branch fractures," in *Paper SPE 162515-MS Presented at the SPE Canadian Unconventional Resources Conference*, Calgary, Alberta, Canada, 2012.

[15] B. Xu, M. Haghighi, X. Li, and D. Cooke, "Development of new type curves for production analysis in naturally fractured shale gas/tight gas reservoirs," *Journal of Petroleum Science and Engineering*, vol. 105, pp. 107–115, 2013.

[16] J. A. Afsar, S. Shahab, and D. Hassan, "Analyzing the production data of fractured horizontal wells by a linear triple porosity model: development of analysis equations," *Journal of Petroleum Science and Engineering*, vol. 112, pp. 117–128, 2013.

[17] F. J. Medeiros, E. Ozkan, and H. A. Kazemi, "Semianalytical approach to model pressure transients in heterogeneous reservoirs," *SPE Reservoir Evaluation & Engineering*, vol. 13, no. 2, pp. 341–358, 2010.

[18] M. Nobakht and C. R. Clarkson, "A new analytical method for analyzing linear flow in tight/shale gas reservoirs: constant-flowing-pressure boundary condition," *SPE Reservoir Evaluation & Engineering*, vol. 15, no. 3, pp. 370–384, 2013.

[19] M. Nobakht, C. R. Clarkson, and D. Kaviani, "New type curves for analyzing horizontal well with multiple fractures in shale gas reservoirs," *Journal of Natural Gas Science and Engineering*, vol. 10, pp. 99–112, 2013.

[20] M. Nobakht, L. Mattar, S. Moghadam, and D. M. Anderson, "Simplified forecasting of tight/shale gas production in linear flow," *Journal of Canadian Petroleum Technology*, vol. 51, no. 6, pp. 476–486, 2013.

[21] E. Stalgorova and L. Mattar, "Analytical model for unconventional multifractured composite systems," *SPE Reservoir Evaluation & Engineering*, vol. 16, no. 3, pp. 246–256, 2013.

[22] W. Luo, C. Tang, Y. Zhou, B. Ning, and J. Cai, "A new semi-analytical method for calculating well productivity near discrete fractures," *Journal of Natural Gas Science and Engineering*, vol. 57, pp. 216–223, 2018.

[23] M. Wei, J. Liu, D. Elsworth, and E. Wang, "Triple-porosity modelling for the simulation of multiscale flow mechanisms in shale reservoirs," *Geofluids*, vol. 2018, Article ID 6948726, 11 pages, 2018.

[24] B. Yuan, G. R. Moghanloo, and D. Zheng, "A novel integrated workflow for evaluation, optimization, and production predication in shale plays," *International Journal of Coal Geology*, vol. 180, pp. 18–28, 2017.

[25] D. Zheng, B. Yuan, and R. G. Moghanloo, "Analytical modeling dynamic drainage volume for transient flow towards multi-stage fractured wells in composite shale reservoirs," *Journal of Petroleum Science and Engineering*, vol. 149, pp. 756–764, 2017.

[26] Y. M. Cheng, "Pressure transient characteristics of hydraulically fractured horizontal shale gas wells," in *Paper SPE 149311 Presented at the SPE Eastern Regional Meeting*, Columbus, Ohio, 2011.

[27] F. Dongyan, Y. Jun, S. Hai, Z. Hui, and W. Wei, "A composite model of hydraulic fractured horizontal well with stimulated reservoir volume in tight oil & gas reservoir," *Journal of Natural Gas Science and Engineering*, vol. 24, pp. 115–123, 2015.

[28] C. M. Freeman, G. J. Moridis, D. Ilk, and T. A. Blasingame, "A numerical study of performance for tight gas and shale gas reservoir systems," in *SPE Paper 124961 Presented at the SPE Annual Technical Conference and Exhibition*, USA, New Orleans, Louisiana, 2009.

[29] D. Li, C. Xu, J. Y. Wang, and D. Lu, "Effect of Knudsen diffusion and Langmuir adsorption on pressure transient response in tight- and shale-gas reservoirs," *Journal of Petroleum Science and Engineering*, vol. 124, pp. 146–154, 2014.

[30] D. Li, L. Zhang, J. Y. Wang, and D. Lu, "Composition-transient analysis in shale-gas reservoirs with consideration of multicomponent adsorption," *SPE Journal*, vol. 21, no. 2, pp. 648–664, 2016.

[31] W. Luo, X. Wang, C. Tang, Y. Feng, and E. Shi, "Productivity of multiple fractures in a closed rectangular reservoir," *Journal of Petroleum Science and Engineering*, vol. 157, pp. 232–247, 2017.

[32] V. Mongalvy, E. Chaput, S. Agarwal, and L. Lu, "A new numerical methodology for shale reservoir performance evaluation," in *Paper SPE 144154 Presented at the North American Unconventional Gas Conference and Exhibition*, The Woodlands, Texas, USA, 2011.

[33] W. Yu and K. Sepehrnoori, "Simulation of gas desorption and geomechanics effects for unconventional gas reservoirs," *Fuel*, vol. 116, pp. 455–464, 2014.

[34] R. H. Zhang, L. H. Zhang, R. H. Wang, Y. L. Zhao, and D. L. Zhang, "Research on transient flow theory of a multiple fractured horizontal well in a composite shale gas reservoir based on the finite-element method," *Journal of Natural Gas Science and Engineering*, vol. 33, pp. 587–598, 2016.

[35] R. H. Zhang, L. H. Zhang, R. H. Wang, Y. L. Zhao, and R. Huang, "Simulation of a multistage fractured horizontal well with finite conductivity in composite shale gas reservoir through finite-element method," *Energy & Fuels*, vol. 30, no. 11, pp. 9036–9049, 2016.

[36] Y. L. Zhao, L. H. Zhang, and B. C. Shan, "Mathematical model of fractured horizontal well in shale gas reservoir with rectangular stimulated reservoir volume," *Journal of Natural Gas Science and Engineering*, vol. 59, pp. 67–79, 2018.

[37] S. Yao, F. Zeng, H. Liu, and G. Zhao, "A semi-analytical model for multi-stage fractured horizontal wells," *Journal of Hydrology*, vol. 507, pp. 201–212, 2013.

[38] H. K. Nie and J. C. Zhang, "Types and characteristics of shale gas reservoir: a case study of Lower Paleozoic in and around Sichuan Basin," *Petroleum Geology & Experiment*, vol. 33, no. 3, pp. 219–232, 2011.

[39] B. Song, *Pressure transient analysis and production analysis for New Albany shale gas wells*, Master Thesis, Texas A & M University, Texas, USA, 2010.

[40] Y. Zhao, L. Zhang, Y. Xiong, Y. Zhou, Q. Liu, and D. Chen, "Pressure response and production performance for multi-fractured horizontal wells with complex seepage mechanism in box-shaped shale gas reservoir," *Journal of Natural Gas Science and Engineering*, vol. 32, pp. 66–80, 2016.

[41] R. G. Loucks, R. M. Reed, S. C. Ruppel, and U. Hammes, "Spectrum of pore types and networks in mudrocks and a descriptive classification for matrix-related mudrock pores," *AAPG Bulletin*, vol. 96, no. 6, pp. 1071–1098, 2012.

[42] F. Sun, Y. Yao, G. Li et al., "A slip-flow model for oil transport in organic nanopores," *Journal of Petroleum Science and Engineering*, vol. 172, pp. 139–148, 2018.

[43] F. Sun, Y. Yao, G. Li, and X. Li, "Transport zones of oil confined in lipophilic nanopores: a technical note," *Arabian Journal of Geosciences*, vol. 12, no. 4, p. 136, 2019.

[44] H. Singh, F. Javadpour, A. Ettehadtavakkol, and H. Darabi, "Nonempirical apparent permeability of shale," *SPE Reservoir Evaluation Engineering*, vol. 17, no. 3, pp. 414–424, 2014.

[45] H. Singh and F. Javadpour, "Langmuir slip-Langmuir sorption permeability model of shale," *Fuel*, vol. 164, pp. 28–37, 2016.

[46] T. Huang, L. Cao, C. Yuan, and P. Chen, "A novel numerical model of gas transport in multiscale shale gas reservoirs with considering surface diffusion and Langmuir slip conditions," *Energy Science Engineering*, vol. 7, no. 4, pp. 1315–1332, 2019.

[47] M. Naraghi, F. Javadpour, and L. T. Ko, "An object-based shale permeability model: non-Darcy gas flow, sorption, and surface diffusion effects," *Transport in Porous Media*, vol. 125, no. 1, pp. 23–39, 2018.

[48] F. Sun, Y. Yao, G. Li, and X. Li, "A slip-flow model for multi-component shale gas transport in organic nanopores," *Arabian Journal of Geosciences*, vol. 12, no. 5, p. 143, 2019.

[49] S. Brunauer, L. S. Deming, W. E. Deming, and E. Teller, "On a theory of the van der Waals adsorption of gases," *Journal of the American Chemical Society*, vol. 62, no. 7, pp. 1723–1732, 1940.

[50] Y. L. Zhao, L. H. Zhang, J. Z. Zhao, J. X. Luo, and B. N. Zhang, ""Triple porosity" modeling of transient well test and rate decline analysis for multi-fractured horizontal well in shale gas reservoirs," *Journal of Petroleum Science and Engineering*, vol. 110, pp. 253–262, 2013.

[51] T. Wu and S. Wang, "A fractal permeability model for real gas in shale reservoirs coupled with Knudsen diffusion and surface diffusion effects," *Fractals*, vol. 28, no. 1, p. 2050017, 2020.

[52] L. H. Zhang, Z. X. Chen, and Y. L. Zhao, *Well Production Performance Analysis for Shale Gas Reservoirs*, Elsevier, Cambridge, United States, 2019.

[53] X. H. Tan, J. Y. Liu, X. P. Li, L. H. Zhang, and J. Cai, "A simulation method for permeability of porous media based on multiple fractal model," *International Journal of Engineering Science*, vol. 95, pp. 76–84, 2015.

[54] Y. Wang and X. Y. Yi, "Transient pressure behavior of a fractured vertical well with a finite-conductivity fracture in triple media carbonate reservoir," *Journal of Porous Media*, vol. 20, no. 8, pp. 707–722, 2017.

[55] A.-R. Salam, "Performance-based comparison for hydraulically fractured tight and shale-gas reservoirs with and without non-Darcy-flow effect," *SPE Reservoir Evaluation & Engineering*, vol. 4, pp. 981–1006, 2018.

[56] M. K. Fisher, C. A. Wright, B. M. Davidson et al., "Integrating fracture mapping technologies to optimize stimulations in the Barnett shale," in *Paper SPE 77441-MS Presented at Annual Technical Conference and Exhibition*, San Antonio, Texas, USA, 2002.

[57] M. Mayerhofer, E. P. Lolon, and N. Warpinski, "What is stimulated rock volume?," in *Paper SPE 119890-MS Presented at SPE Shale Gas Production Conference, 16-18 November*, Fort Worth, Texas, USA, 2008.

[58] Y. L. Zhao, L. H. Zhang, J. X. Luo, and B. N. Zhang, "Performance of fractured horizontal well with stimulated reservoir volume in unconventional gas reservoir," *Journal of Hydrology*, vol. 512, pp. 447–456, 2014.

[59] K. Sato and R. N. Horne, "Perturbation boundary element method for heterogeneous reservoirs: part 1: steady-state flow problems," *SPE Formation Evaluation*, vol. 8, no. 4, pp. 306–314, 2013.

[60] K. Sato and R. N. Horne, "Perturbation boundary element method for heterogeneous reservoirs: part 2—transient-flow problems," *SPE Formation Evaluation*, vol. 8, no. 4, pp. 315–322, 1993.

[61] Y. Zhao, H. Li, L. Zhang, and B. Kang, "Pressure transient analysis for off-centered fractured vertical wells in arbitrarily shaped gas reservoirs with the BEM," *Journal of Petroleum Science and Engineering*, vol. 156, pp. 167–180, 2017.

[62] Y. L. Zhao, B. C. Shan, L. H. Zhang, and Q. G. Liu, "Seepage flow behaviors of multi-stage fractured horizontal wells in arbitrary shaped shale gas reservoirs," *Journal of Geophysics and Engineering*, vol. 13, no. 5, pp. 674–689, 2016.

[63] A. R. Salam and E. A. Fazil, "How much stimulated reservoir volume and induced matrix permeability could enhance unconventional reservoir performance," *Journal of Natural Gas Science and Engineering*, vol. 46, pp. 764–781, 2017.

[64] A.-R. Salam, "Productivity-index behavior for hydraulically fractured reservoirs depleted by constant production rate

considering transient-state and semisteady-state conditions," *SPE Production & Operations*, vol. 33, no. 4, 2018.

[65] J. Guo, Y. Li, J. Zhao, and Y. Ren, "The application of boundary element method to pressure behavior analysis in a composite reservoir with lateral drilling," *Journal of Canadian Petroleum Technology*, vol. 43, no. 7, pp. 38–44, 2004.

[66] K. Jongkittinarukorn, D. Tiab, and F. H. Escobar, "Interpretation of horizontal well performance in complicated systems by the boundary element method," in *Paper SPE50437-MS Presented at the SPE International Conference on Horizontal Well Technology*, Calgary, Alberta, Canada, 1998.

[67] J. Kikani and R. N. Horne, "Modeling pressure-transient behavior of sectionally homogeneous reservoirs by the boundary-element method," *SPE Formation Evaluation*, vol. 8, no. 2, pp. 145–152, 2013.

[68] L. S. Koh and D. Tiab, "3D. Boundary-element model for predicting performance of horizontal wells," in *Paper SPE 26101-MS Presented at the SPE Western Regional Meeting, 26-28 May*, Anchorage, Alaska, USA, 1993.

[69] W. Sung, W. Lee, and I. Kim, "Development and validation of interference testing analysis model using boundary element method for geometrically complex reservoirs," in *Paper SPE 54272-MS Presented at the SPE Asia Pacific Oil and Gas Conference and Exhibition*, Jakarta, Indonesia, 1999.

[70] H. T. Wang and L. H. Zhang, "A boundary element method applied to pressure transient analysis of geometrically complex gas reservoirs," in *Paper SPE 122055-MS Presented at the Latin American and Caribbean Petroleum Engineering Conference*, Cartagena de Indias, Colombia, 2009.

[71] L. H. Zhang, C. Y. Li, and Q. G. Liu, "The application of boundary element theory about seepage in complex boundary reservoir in horizontal wells," *Computational Mechanics*, vol. 26, no. 2, pp. 287–290, 2009.